Proceedings of the ASME 2022 17th International Manufacturing Science and Engineering Conference
MSEC2022
June 27-July 1, 2022, West Lafayette, Indiana, USA

MSEC2022-85424

MACHINE VISION TRACKING AND AUTOMATION OF A MICROROBOT (SAFAM)

Colin Warn,[1] Andriy Sherehiy[2], Moath Alqatamin[2], Brooke Ritz[2], Ruoshi Zhang[2], Sri S Chowdhury[2], Danming Wei[2], Dan O. Popa[2]

[1]Department of Mechanical Engineering, Washington State University, Pullman, Washington.
[2]Louisville Automation and Robotic Research Institute (LARRI), University of Louisville, Louisville, Kentucky.

ABSTRACT

In this paper, we propose a method for tracking a microrobot's three-dimensional position using microscope machine vision. The microrobot, theSolid Articulated Four Axis Microrobot (sAFAM), is being developed to enable the assembly and manipulation of micro and nanoscale objects. In the future, arrays of sAFAMS working together can be integrated into a wafer-scale nanofactory, Prior to use, microrobots in this microfactory need calibration, which can be achieved using the proposed measurement technique. Our approach enables faster and more accurate mapping of microrobot translations and rotations, and orders of magnitude larger datasets can be created by automation. Cameras feeds on a custom microscopy system is fed into a data processing pipeline that enables tracking of the microrobot in real-time. This particular machine vision method was implemented with a help of OpenCV and Python and can be used to track the movement of other micrometer-sized features. Additionally, a script was created to enable automated repeatability tests for each of the six trajectories traversable by the robot. A more precise microrobot workable area was also determined thanks to the significantly larger datasets enabled by the combined automation and machine vision approaches.
Keywords: Micro robotics, machine vision, nano microscale manufacturing.

1. INTRODUCTION

Manipulation of the micro and nanoscopic objects, in a reliable and precise manner, is fundamental for nano-microscale manufacturing. It is especially important in the case of the direct handling of the individual structures which can be realized with the help of microscopic robots and robotic arms. A number of the numerous solutions were proposed Microscopic robots and robotic arms. Recently numerous solutions were explored regarding microscale robots with a different type of actuation [1 - 3], and advances were made concerning precision and reliability [1,4]. Integration of the microscopic robots as part of the micro-factory concept introduced a new class of challenges. Specifically, automation with an open/closed-loop control requires awareness of the robot's behavior, for example, the location of its components, realized with the help of sensing or visual feedback. Automation with the help of vision processing is especially feasible when microrobots are used for manipulation tasks in situ optical microscopes or Scanning Electron Microscopes (SEM) [5]. Different vision processing solutions were proposed so far including virtual environment to facilitate teleoperation of AFM cantilever in situ SEM [6], Chu et. al. implemented path planning with the assistance of vision processing for manipulation of multiple microscale spheres [7], vision serving was used for tracking of the laser-driven microrobot during its motion [2,3].

A combination of magnetic and electrostatic controls has been developed to realize the motion of modern microscale robots [8-10]. Fabrication of many microrobots uses integrated circuit (IC) or microelectromechanical system (MEMS) techniques. The Articulated Four Axis Robot (AFAM) is one instance of the MEMS-derived robot family, enabling "out-of-plane" manipulation (three-dimensional manipulation, in contrast to the two-dimensional "in-plane" manipulation) [11]. AFAM is built using Zyvex® connectors, a snap fastener-style MEMS coupling device which greatly reduces the effort needed to perform micro-assembly tasks [12,13].
Afam however, experienced coupling and assembly challenge upon design and implementation. for instance, the cable experienced a higher than desired fatigue failure. to reduce these problems, a second-generation afam device was designed, known as a solid articulated four axis microrobot (safam) [14]. this improved the afam design by rotating the zyvex connector 90 degrees while adding a more fatigue-resistant supporting

beam and thin beam spring the reported capabilities of the microrobot in our earlier studies potentially enable the realization of the manipulation of nano/microscale objects, e.g. demonstrated custom control solution for remote manipulation of sAFAM by a human operator [8].

This paper discusses the implementation of machine vision-powered software to expedite the speed of testing and calibrated operation of the sAFAM. To this end, an experimental setup was implemented and used to acquire a live video feed of the microrobot tip motion from two perpendicularly placed cameras. Machine vision tracking was used to image the motion automatically, and data were collected to evaluate the repeatability and workspace of the microrobot [9-11]. Custom software using OpenCV and Python was implemented, and experimental results measuring the robot's workspace and repeatability were obtained. Results indicate that the sAFAM has a workspace of approximately X: 80 µm, Y: 35 µm, Z:100 µm, and a motion repeatability of approximately minimum value of 0.5 µm and maximum value of 26 µm.

Our paper is organized in the following way: in Section 2, we briefly describe sAFAM (design, fabrication, assembly). control system and its tools. The experimental setup is described in section 3. Section 4 presents the machine vision tracking solution. Then in section 5, we discuss experimental data and future work. Finally, we conclude the paper.

2. MICROROBOT DESCRIPTION AND OPERATION

The following is a description of sAFAM, as well as the electronical components that enable its manipulation.

2.1 Hardware and Manipulation Overview

Solid Articulated Four-Axis Microrobot (sAFAM) is designed to carry out robotic manipulation tasks in micro and nanometer scales with or without a human operator in the loop. It replaces the need for conventional mesoscale manipulators, and when produced in large quantities, a group of sAFAMs can be deployed in a desktop microfactory to fulfill a series of automated micro-assembly tasks with the help of smart control algorithms.

The sAFAM is assembled from two main components: An in-plane base with four MEMS thermal actuators, and an assembled out-of-plane monolithic manipulator. These can be seen in Figure 2. Each electrothermal actuator is labeled ("A", "B", "C", and "D"), and each has ten individual long and thin beams placed in a parallel and symmetric manner. Each beam measures 16 µm wide, 2000µm long, and 100µm deep. On the side of the base, there are 6 gold-plated contact pads to supply electrical current to the actuators, marked from 1 to 6 in Figure 1. The shuttle of each thermal actuator is extended and connected to a centerpiece, which offers a mechanical connection to the out-of-plane manipulator arm to be assembled. Four supporting springs with very low spring constants are connected to the corner of the centerpiece to balance actuation force. Through a "Zyvex" snap-fastener, the manipulator arm can be assembled onto the base with the help of a special micro end-effector. The manipulator's arm employs a two-spring structure as "transmission" to convert the in-plane motion to out-of-plane and eventually to the end-effector [8].

sAFAM is fabricated in a cleanroom with standard MEMS fabrication procedures. We chose silicon-on-insulator (SOI) wafers as the substrate for the device, in tandem with buried oxide (BOX), and handle layer thickness of 100µm, 2µm, and 500µm respectively. The substrate is first cleaned with the RCA cleaning procedure, after which a thin layer of gold with chromium as an adhesion layer is deposited as the electrical contacts. The Lesker PVD-75 sputterer is tuned to 300W DC for 2 minutes and 4 minutes for chromium and gold, respectively. Next, the contact pattern is transferred through Shipley 1813 photoresist onto the metal, which is etched by corresponding etchant. The first photoresist is then removed, and the SPR220-3.0 photoresist is spin-coated and patterned as an etching mask for the features of the in-plane base, the out-of-plane manipulator arm, as well as the special micromanipulator that is used to assemble the two. The deep reactive ion etching (DRIE) process eventually carves out the body of the parts for sAFAM. After dicing, desired dies are released in the vapor HF etching tool, and they are ready to be assembled [8,14].

Figure 1 shows the 3D CAD model of the sAFAM system. Any tooling that is mounted to sAFAM is mounted to the end effector, as pointed to in the image. The end effector's position is manipulated by four actuators, labeled A, B, C, and D in Figure 2. Also shown in the figure are six gold-plated PCB pads. A voltage is applied across two of these pads, which leads to electrostatic manipulation of a given actuator. For instance, if the voltage is applied between pads 2 and 3 as shown in the photo, Actuator A is moved. The actual pad to actuator pinout is shown below. Note that the pin order is listed from right to left as the PCB headers are connected from right to left.

TABLE 1: SAFAM PINOUT TABLE.

Pin	6	5	4	3	2	1
Actuator	A	C	D	(GND)	B	(GND)

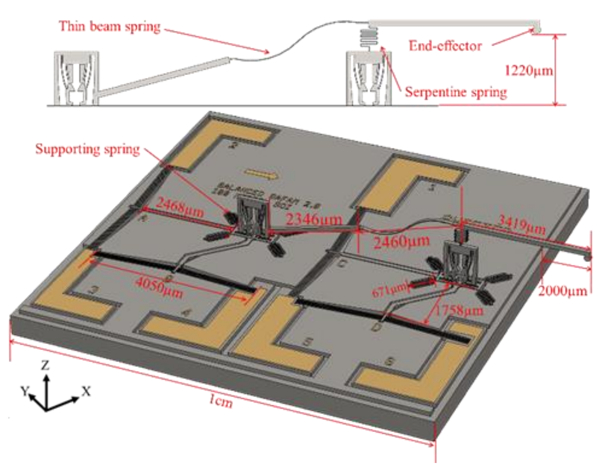

FIGURE 1: SAFAM 3D MODEL.

Each actuator is linearly translated using a voltage applied between two pads. A translation in one actuator leads to a corresponding movement of the end effector. For instance, If either A and C or B and D actuators move by the same amount, this leads to translational motion for the end effector on a given axis. Individual actuator movement leads to the end effector either pitching or yawing. Further details can be found in Alqatamin et. al's paper [8].

3. EXPERIMENTAL SETUP

A schematic of the sAFAM electrical control system and user interface was described in detail in a previous publication [8]. The following components which make up the control system include a TI USB2ANY interface adapter, an Arduino Uno, a development board, a buffer amplifier, and a programmable power supply. The Arduino serves as the serial translator between the user's laptop and the development board's Digital to Analog Converter. The Arduino connects directly to the user's laptop, allowing the user to command voltages directly to sAFAM using a Python script.

The User Interface also integrated a Logitech Flight Simulator Joystick as well as an Xbox controller as a means of control.

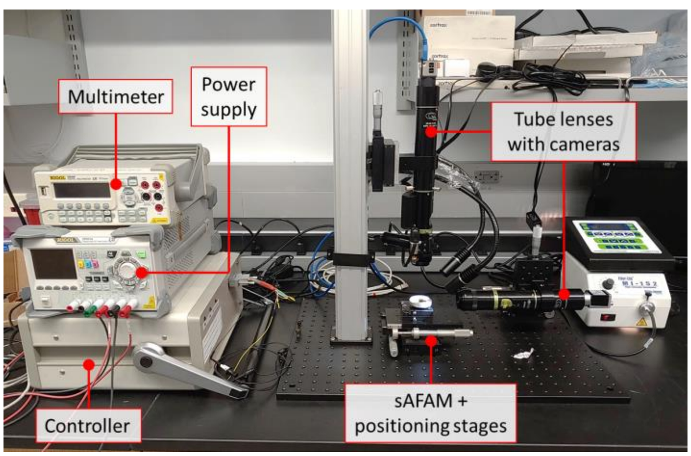

FIGURE 2 EXPERIMENTAL TEST SETUP [8].

4. MACHINE VISION REAL-TIME TRACKING

To characterize the microrobot tip motion, a real-time vision system was implemented into the experimental setup. The system, programmed in Python, uses OpenCV's Discriminative Correlation Filter with Channel and Spatial Reliability Tracker (CSRT for short) algorithm to track the movement of Sadam's end effector. Other tracking algorithms such as Kernelized Correlation Filters (KCFs) and the Minimum Output Sum of Squared Error (MOSSE) trackers were tried but were not able to track the end effector as consistently as the CSRT algorithm [15]. The KCF algorithm, when applied, would lose the lock of the microrobot after several actions. MOSSE, though it could keep a lock of the microrobot, was not as accurate as CSRTs were in determining the active position of the robot. Previous literature has explored using machine vision to track robots with millimeter precision, however it is an open question whether these techniques can extend down to the micrometer range.[16]

Figure 2 shows CEFAM's experimental test setup. Two cameras are placed orthogonally to each other over the microrobot. The resolution of the top and side cameras were 0.125 and 0.5 microns per pixel respectively, resolutions which were used as conversion factors. It is noted that the system is not mounted on a vibration-tolerant table and was stationed in a laboratory with moderate levels of human activity. Better resolution should be found by placing the setup in something like a Scanning Electron Microscope (SEM).

The abounding box is drawn by the user around the desired object to track, as shown in Figure 3. This bounding box's origin is defined around the bound box's central pixel, as shown by the dot in the picture. The coordinates of this reference frame in units of pixels are defined concerning the camera's reference frame in the top left at point (0,0). Any translation of the box's origin concerning the camera's reference frame defines the live position of the bounding box. In Figure 3 for example, the live position of the bounding box (3,4) is 3 pixels to the right and 4 pixels down concerning the camera. Using the process described in previous papers [8], a pixel to micrometer displacement coefficient can be determined.

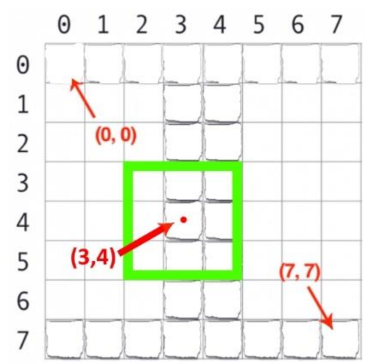

FIGURE 3 OPENCV BOUNDING BOX EXAMPLE. UNITS ARE IN PIXELS. [17]

The author notes that this coefficient is the limiting factor in the accuracy of this process. With increased camera resolution, the displacement coefficient decreases, and this method's accuracy increases.

As shown in Figure 6, when two cameras are perpendicularly placed to each other, each with their separate bounding boxes around the object, live 3D position data can be displayed. CEFAM's end effector coordinate frame is defined by the centers of these bounding boxes. Factors such as object defocusing occlusion are handled by the OpenCV backend. A video of the tracking system in action can be found in the following reference [18,19].

4.1 Workflow

When the program is initially executed, the user is prompted to supply a numerical conversion factor for the given camera, enabling the program to convert the pixel X and Y position outputs to a micrometer position output. The user is then prompted to draw the bounding box around the desired object to be tracked. Steps 1 and 2 are then repeated for the next camera. The final output will look something like the following.

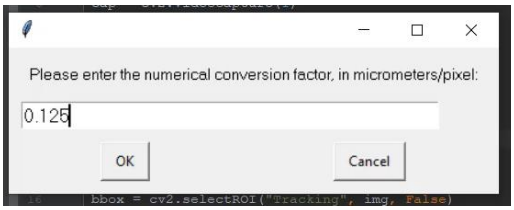

FIGURE 4 (STEP 1) GETS THE CONVERSION FACTOR FOR THE GIVEN CAMERA.

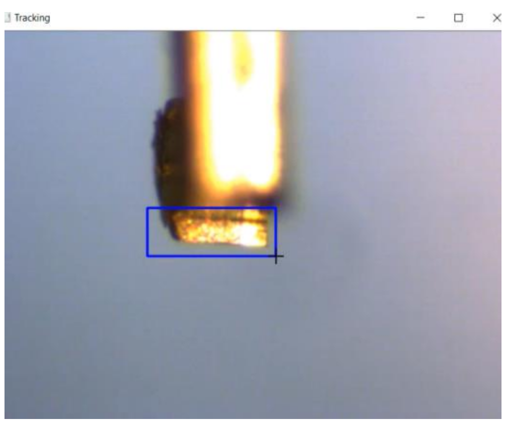

FIGURE 5 (STEP 2) GETS THE CONVERSION FACTOR FOR THE GIVEN CAMERA.

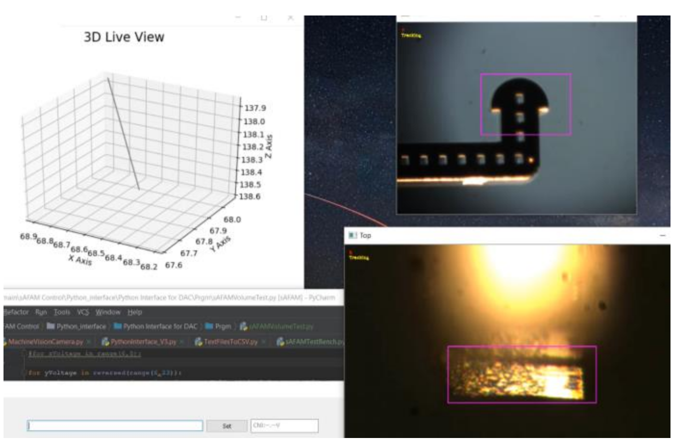

FIGURE 6 (STEP 3) TOP AND SIDE VIEW OUTPUT.

4.2 Automation

Previous work required the user to manually input voltages to maneuver the microrobot to desired locations. In the previous code, voltages could only be set through a PyQt5 form. To make this process more automated, custom Python code was created on top of the PyQt5 code to enable manipulation of the robot without requiring direct human input. Section 5 describes the automated tests that were performed thanks to this code.

5. EXPERIMENTAL RESULTS AND DISCUSSION

Two groups of tests were performed as part of this research: sAFAM end effector displacement as a function of voltage, and sAFAM end-effector position city as a function. The former of these is straightforward to understand (how far along what axis oes the end effect tor move for a given voltage), but these pants a quick explore action.

Position Repeatability (RR): Closeness of agreement between the measured (attained) position after n repeat visits to the same commanded position. [8,19]

$$R_R = \bar{l} + 3S_l \tag{1}$$

Where

$$\bar{l} = \frac{1}{n}\sum_{k=1}^{n} l_k \tag{2}$$
$$l_k = \sqrt{(x_k - \bar{x})^2 + (y_k - \bar{y})^2 + (z_k - \bar{z})^2}$$

With x, y, z, and x_k, y_k, z_k as defined in 4.3, and

$$S_l = \sqrt{\frac{\sum_{k1}^{n} \left(l_k \bar{l}\right)^2}{n-1}} \tag{3}$$

and x_k, y_k, and z_k - coordinates of the k-th attained pose; and n= number of measurement samples.

This definition of repeatability is what previous sAFAM work has been used to codify the precision of its robotic arm movement. The following tests were performed for the robot.

5.1 Linear Step Test

Displacement values were measured in a range of 6 to 22 V for each trajectory of the robot (see Figure 4: X translation, Y translation, etc.). Each voltage value in this range was visited ten times in a row in 1 V increments. Four seconds wait times between each voltage value were programmed into the automation process. Displacement versus voltage and repeatability versus voltage measurements were recorded (Figure 7 and 8). Except for translation along the X-axis, all trajectories seemed to minimize position repeatability while maximizing end effector displacement between 10 and 15 V. It is therefore recommended that the robot be run in between these voltage values for all the degrees of freedom except the X-axis. Repeatability measurements revealed that the most optimal mode of Sadam's operation is for the actuation voltage in the range 10 – 15 V for all the degrees of freedom (Figure 8). In this range distribution of the repeatability values is the most narrow. The minimum value of repeatability was recorded for the pitch up motion – 0.5 μm and the maximum for the X translational motion – 26 μm. We have observed a visible trend where repeatability is increasing with voltage. The exception is X and Y translational motion in the range 5.5 – 8 V for which repeatability values are much higher compared to the pitch and yaw and are decreasing with the voltage. However, above 9 V XY repeatability follows a general trend.

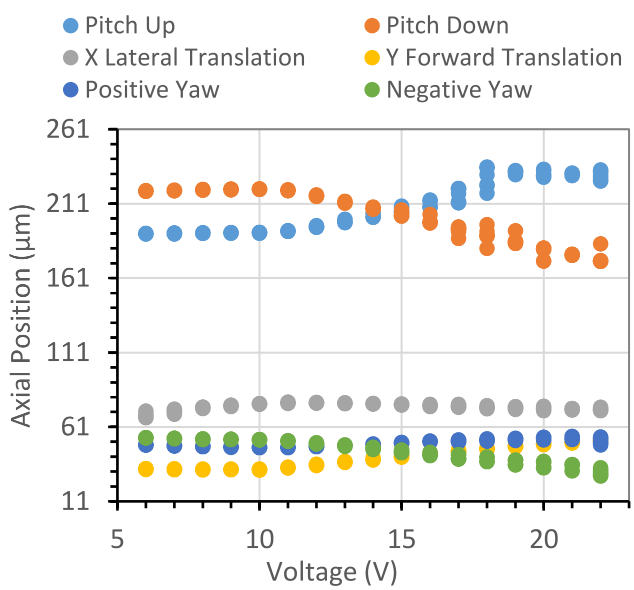

FIGURE 7 DISPLACEMENT VERSUS VOLTAGE FOR EACH ACTUATION MOVEMENT.

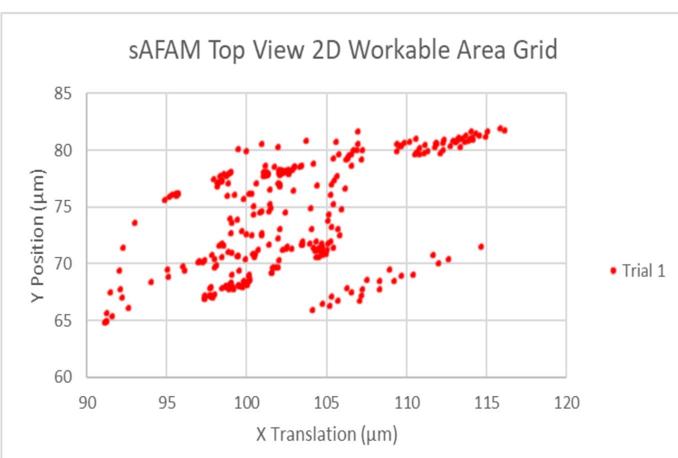

FIGURE 9 2D LINEAR STEP TEST DATA.

This behavior might be related to the fact that motion in X or Y directions is realized with the help of two actuators whereas only one is used for pitch and yaw motion.

5.2 2D Linear Step Test

Using the X translation and Y translation trajectories, a 2D grid of data points was created with sAFAM end effector actuation in 1V increments to determine the 2D linear uniformity of sAFAM end effector movements. It is observed from this data that the lines are not as straightforward as one would expect due to thermal coupling between the actuator pads.

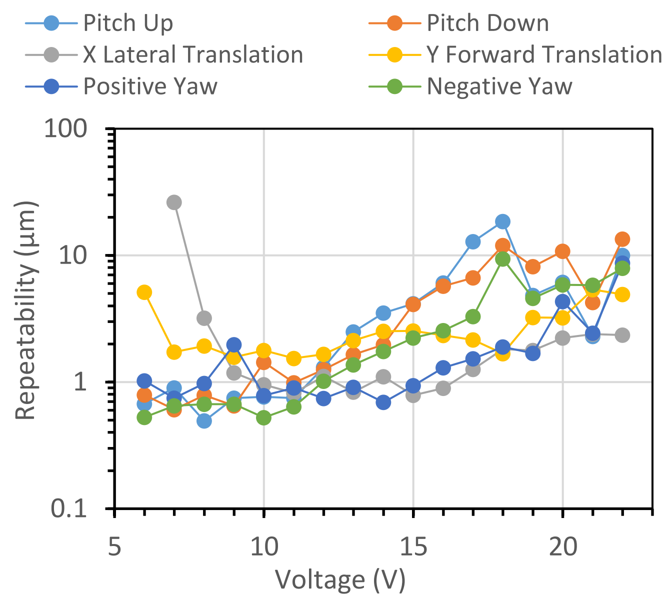

FIGURE 8 REPEATABILITY MEASUREMENTS FOR EACH ACTUATOR.

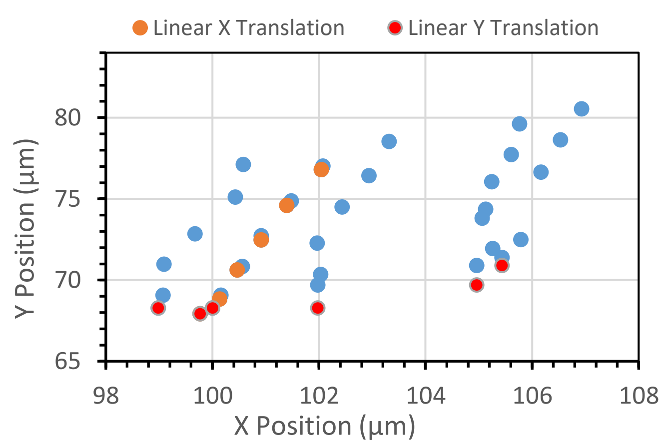

FIGURE 10 2D LINEAR STEP TEST DATA, FROM 10-15V

Outside of the 10-15V range, the 2D Linear Step Test showed strongly nonlinear outputs. It is also noted by the author that micrometer levels of camera misalignment could be contributing to the nonlinear patterns being shown in Figures 10 and 11. The addition of an inclinometer to the setup would help determine contributions of camera misalignment and thermal coupling to the skewed-looking results shown in Figure 11.

5.3 3D Workspace Mapping

A 3D map of the sAFAM end effector workspace was created. The four actuator pads received random voltages between 6 and 22 V in 1V step sizes. 2000 data points were taken from combinations of these voltages to yield this final map. The approximate dimensions of this workspace, derived from Figure 11, are as follows:X-axis: 80 µm, Y-axis: 35 µm, Z-axis 100 µm.

5.4 Time-limited Repeatability Trend

The linear negative yaw displacement test was run for eight seconds to determine whether end effector repeatability would improve. Doubling the wait time seemed to slightly improve the average positional repeatability for each voltage, as shown in table #2 and Figure 12. This behavior was observed in earlier studies and is explained by the properties of the electrothermal chevron actuators [8,14]. Since the operation principle of chevron actuators is based on Joule's heating, when the voltage is applied or not, expansion-contraction of the structures is subjected to delay until it reaches equilibrium. This effect is in turn translated onto the sAFAM's arm motion and amplified when actuators are engaged.

5.4 Future work - Testing Inside of a Scanning Electron Microscope

As mentioned in the experimental setup section of this paper the machine-vision-based approach can be improved by mounting the microrobot on a vibration-resistant table with better camera resolution. A scanning electron microscope is such a technology where, if this experiment methodology were implemented, should yield better precision results than reported in this writeup.

Given data sets with thousands of data points can be created in as little as a few hours, an inverse model mapping the desired sAFAM end-effector location to the required voltages can now be created.

A lookup table, combined with interpolation, is suggested by the author as the most promising path forward for this line of research. n easier method of interfacing with this model, such as integration with Robot Operation System software, should also be undertaken.

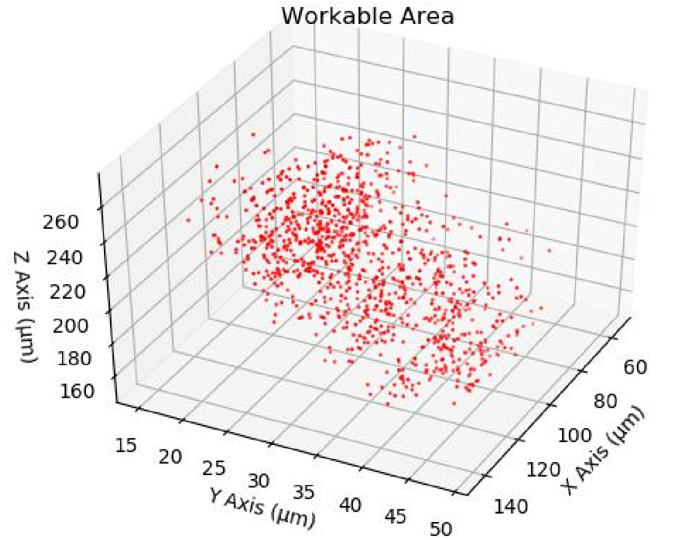

FIGURE 11 3D MAP OF SAFAM END EFFECTOR WORKSPACE.

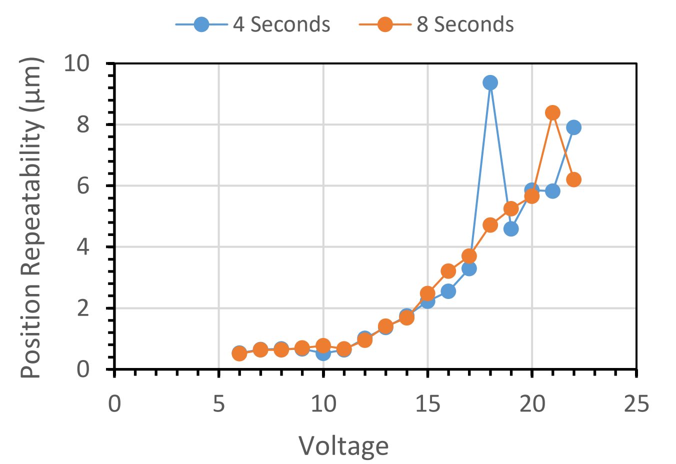

FIGURE 12 POSITION REPEATABILITY AS A FUNCTION OF DELAY TIME BETWEEN SAFAM ACTUATIONS.

TABLE 2: MEAN AND STANDARD DEVIATIONS OF VALUES FROM FIGURE 19.

Axis	4 Second Positional Repeatability Mean	4 Second Positional Repeatability STD	8 Second Positional Repeatability Mean	8 Second Positional Repeatability STD
Negative Yaw	3.08	2.95	2.94	2.56

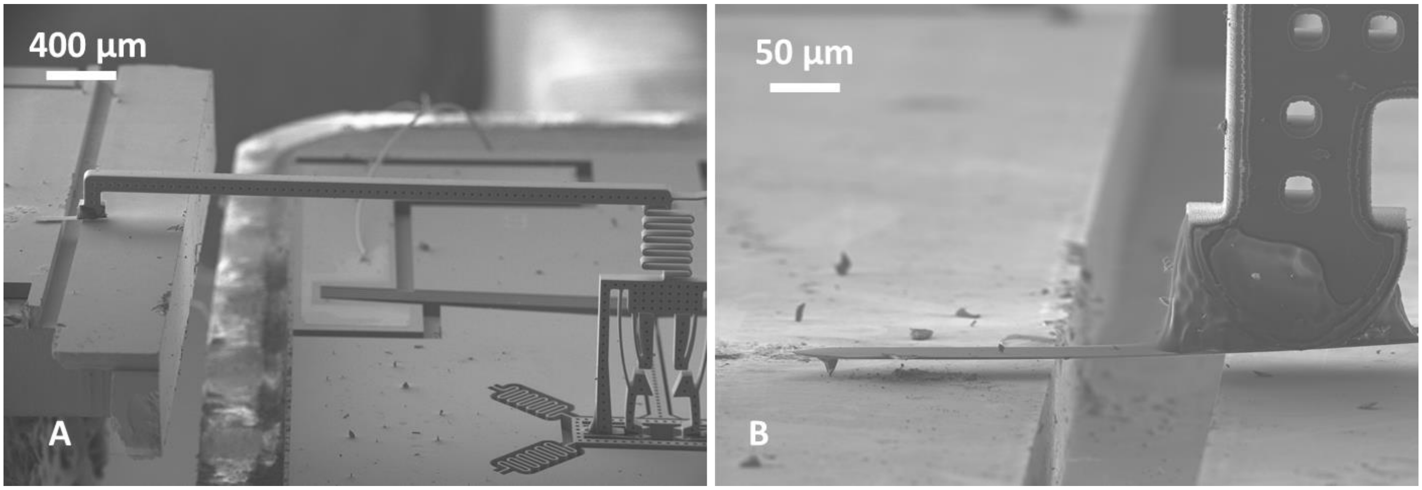

FIGURE 13 SEM image of sAFAM arm in situ SEM: A) general view of the sAFAM arm with end effector and Zyvex component; B) detail of the sAFAM's arm end effector with attached AFM cantilever touchin the substrate.

Lastly, developed machine-vision tracking can be implemented for future in situ SEM experiments with sAFAM (Figure 13). In such an arrangement sAFAM's end effector with attached AFM cantilever can be tracked during manipulation tasks of the nano/microscopic objects allowing better control, improved precision, and implementation of the path planning algorithms.

6. CONCLUSION

An automated method of actuating and recording sAFAM end-effector position in three dimensions as a function of voltage has been created using machine vision. This method enables an significantly faster and more precise method of testing, limited only by the resolution of the experimental camera setup. Tests were performed to determine the system's position repeatability for each end-effector trajectory with a minimum value of 0.5 µm and maximum value of 26 µm. A refined workspace (X: 80 µm, Y: 35 µm, Z:100 µm.) map was created to evaluate practical application for the manipulation tasks of sAFAM. In the future developed machine vision method can be applied for the automation of the nano/microscopic objects manipulation tasks in situ SEM.

ACKNOWLEDGEMENTS

The primary author would like to take this moment to especially thank the other co-authors on this paper for their help and patience in putting up with his wild side experiment that led to this paper.

Additional gratitude is extended to the funding sources that enabled this project: NSF Award # 1950137 - REU SITE: Interdisciplinary Micro/nano/additive-manufacturing Program Addressing Challenges Today - Next Generation (IMPACT-NG), and NSF Award #2025075 - NNCI: KY Multiscale.

REFERENCES

[1] C. Jiang, H. Lu, H. Zhang, Y. Shen, and Y. Lu, " Recent Advances on In Situ SEM Mechanical and Electrical Characterization of Low-Dimensional Nanomaterials ", Scanning, Vol. 2017, 1985149, 2017.

[2] Z. Yang, A. Sherehiy, S. S. Chowdhury, D. Wei, R. Zhang, and D. O. Popa, "Design, Fabrication and Experimental Validation of a Steerable, Laser-Driven Microrobot in Dry Environments," in *2020 IEEE 16th International Conference on Automation Science and Engineering (CASE)*, 20-21 Aug. 2020, pp. 882-887, DOI: 10.1109/CASE48305.2020.9216958.

[3] R. Zhang, A. Sherehiy, Z. Yang, D. Wei, C. K. Harnett, and D. O. Popa, "ChevBot – An Untethered Microrobot Powered by Laser for Microfactory Applications," in *2019 International Conference on Robotics and Automation (ICRA)*, 20-24 May 2019, pp. 231-236, DOI: 10.1109/ICRA.2019.8793856.

[4] S. Fatikow, J. Seyfried, S. Fahlbusch, A. Buerkle, and F. Schmoeckel, "A flexible microrobot-based micro-assembly station," in *1999 7th IEEE International Conference on Emerging Technologies and Factory Automation. Proceedings ETFA '99 (Cat. No.99TH8467)*, 18-21 Oct. 1999, vol. 1, pp. 397-406 vol.1, doi: 10.1109/ETFA.1999.815384.

[5] J. Agnus, N. Chaillet, C. Clevy, S. Dembel, M. Gauthier, Y. Haddab, G. Laurent, P. Lutz, N. Piat, K. Rabenorosoa, M. Rakotondrabe, B. Tamadazte, "Robotic microassembly and micromanipulation at FEMTO-ST", J Micro-Bio Robot, 8:91–106, (2013)

[6] Aude Bolopion, Christian Stolle, Robert Tunnell, Sinan Haliyo1, Stephane Regnier and Sergej Fatikow, "Remote

Microscale Teleoperation through Virtual Reality and Haptic Feedback", 2011 IEEE/RSJ International Conference on Intelligent Robots and Systems, 25-30 September, 2011, pp 894-900, doi: 10.1109/IROS.2011.6094453

[7] Henry K. Chua, James K. Mills, William L. Cleghornb, " Automated dual-arm micromanipulation with path planning for micro-object handling", Robotics and Autonomous Systems 74, 166–174, (2015)

[8] M. Alqatamin, B. Ritz, A. Sherehiy, D. Jackson and R. Zhang, "TELEOPERATION INTERFACE FOR SAFAM, A SOLID ARTICULATED FOUR AXES MICROROBOT," in *International Design Engineering Technical Conferences and Computers and Information in Engineering Conference IDETC/CIE2021*, Virtual, Online, 2020.

[9] K. N. N. Y. N. T. Khamesee MB, "Design and control of a micro-robotic system using magnetic levitation.," *IEEE/ASME Transactions on Mechatronics,* vol. 7(1):, p. 1–14, 2002.

[10] T. A. G. S. a. R. D. Karagozler ME, "Electrostatic Actuation and Control of Micro Robots Using a Post-Processed High-Voltage SOI CMOS Chip," in *IEEE International Symposium of Circuits and Systems (ISCAS)*, Rio de Janeiro, Brazil, 2011.

[11] S. H. P. D. Murthy R, "AFAM: an articulated four axes microrobot for nanoscale applications," *IEEE Trans Autom Sci Eng,* no. 10(2), pp. 276-284, 2013.

[12] Tsui K and Geisberger A, "Sockets for micro-assembly". United States Patent US7025619B2,, 13 2 2004.

[13] S. G. a. T. K. Geisberger A, "Micro connectors and non-powered micro-assembly therewith". United States Patent EP1564183A2, 13 2 2004.

[14] R. Zhang, A. Sherehiy, D. Wei and D. O. Popa, "Design and characterization of solid articulated four axes microrobot," *Journal of Micro-Bio Robotics,* 2018.

[15] A. Lukežič, T. Vojíř, L. Čehovin, J. Matas and M. Kristan, "Arxiv," 25 Nov 2016. [Online]. Available: https://arxiv.org/abs/1611.08461.

[16] J. P. Base, S. Yoon, M. Vania and D. Lee, "Three Dimensional Microrobot Tracking Using Learning-based System," *International Journal of Control, Automation and Systems,* vol. 17, pp. 1-8, 2019.

[17] A. Rosebrock, "OpenCV Getting and Setting Pixels," https://www.pyimagesearch.com/, 20 01 2021. [Online]. Available: https://www.pyimagesearch.com/2021/01/20/opencv-getting-and-setting-pixels/. [Accessed 21 7 2021].

[18] C. Warn, "sAFAM Microrobot Machine Vision Tracking," [Online]. Available: https://youtu.be/KM_EVsOubdU. [Accessed 29 11 2021].

[19] T. Zimmerman, "Metrics and Key Performance Indicators for Robotic Cybersecurity Performance Analysis", Gaithersburg, MD: 2019, National Institute of Standards and Technology.